J Mater Sci (2012) 47:479–485
DOI 10.1007/s10853-011-5823-y

Enhancement of photoluminescence due to erbium-doped in CdS thin films

O. Zelaya-Angel · S. A. Tomás · P. Rodríguez · J. G. Mendoza-Alvarez · R. Lozada-Morales · O. Portillo-Moreno · J. González-Hernández

Received: 25 March 2011 / Accepted: 26 July 2011 / Published online: 10 August 2011

Abstract Cadmium sulfide (CdS) thin films were synthesized by chemical bath deposition on glass substrates at 80 °C. The CdS thin films were doped with erbium (Er^{3+}) during the growth process by adding aqueous solutions of $Er(NO_3)_3{\cdot}3H_2O$ to the CdS chemical bath. The relative volume (V_r) of the doping-solution was varied to obtain ten different doping levels. X-ray diffraction patterns displayed the zincblende crystalline structure for all the CdS:Er samples, with a remarked preferred orientation along the (111) direction. The (111) interplanar distance (ID) first decreased, reaching a minimum value at $V_r = 3\%$, after which point it increased up to saturation for largest values of V_r. The dependence of the band-gap energy (E_g) on V_r followed an opposite behavior to that described by the ID. The photoluminescence (PL) spectra showed essentially two main bands: the green emission (GE) band of CdS and a red emission (RE) band. The increasing of the PL signal, for $V_r \leq 4\%$ has been associated with the presence of Er^{3+} into the CdS lattice. For $V_r > 4\%$, Er degrades the lattice. In addition, the crystalline quality (CQ) and PL of the material improved for low V_r values, which was in agreement with measurements of the mobility.

O. Zelaya-Angel · S. A. Tomás · P. Rodríguez · J. G. Mendoza-Alvarez
Departamento de Física, Centro de Investigación y de Estudios Avanzados del IPN, P.O. Box 14-740, México, D.F, Mexico

R. Lozada-Morales (✉)
Facultad de Ciencias Físico-Matemáticas, Benemérita Universidad Autónoma de Puebla, Puebla, Mexico
e-mail: rlozada@fcfm.buap.mx

O. Portillo-Moreno
Facultad de Ciencias Químicas, Benemérita Universidad Autónoma de Puebla, Puebla, Mexico

J. González-Hernández
Centro de Investigación en Materiales Avanzados, Av. Miguel de Cervantes #120, 31109 Chihuahua, Chih, Mexico

Introduction

The doping of semiconductors with rare earth (RE) elements has fascinated researchers over the years because of the potential for electronic and optical applications. Among the most commonly used RE ions, erbium (Er) has been proven successful for light-emitting device applications. The distinguished narrow-line emission associated with the $4f$ intra-transitions of Er^{3+}, as well as the temperature insensitivity of the energy position, has encouraged research in this direction.

Recently, Er^{3+} ions have been successfully incorporated into the core of IV, III–V, and II–VI semiconductors for device fabrication [1–4]. The 1.55 μm emission from an Er-doped GaN LED has been reported by Shen et al. [5] and the excitation and deactivation paths of a Si:Er system have been studied by Gregorkiewicz et al. [6] using a tunable free-electron laser. Er^{3+} has also been used as the active ions in silica-based planar waveguides to get optical amplification and lasing [7]. On the other hand, RE-doped II–VI semiconductors have been studied for their potential use in multicolor cathode-ray tubes and electroluminescent displays [8, 9]. The photoluminescence (PL) of Er-doped ZnSe crystals [10] and of Er^{3+} in p-type ZnSe crystals has been previously investigated [11]. A strong enhancement of the 1.54 μm fluorescence of Er^{3+} has been achieved in highly concentrated II–VI semiconductor quantum dot environments [12]. In addition, Favennec et al. [13] studied a number of Er-doped semiconductors, including Si, InP, GaAs, AlGaAs, GaInAsP, ZnTe, and Cadmium sulfide

(CdS), and proved that the Er^{3+} emission wavelength is essentially constant for semiconductors with band-gap energy greater than the intrashell transition energy of Er 4f electrons, namely, 0.805 eV.

It is well known that CdS exists in either of two different structural phases, namely, a metastable cubic phase and a highly stable hexagonal phase [14]. Cubic phase CdS films display a band-gap shift (BGS) effect that is dependent on the annealing temperature, among other parameters [15]. Subsequently, because of its technological importance in optoelectronic design, the BGS effect of intrinsic and extrinsic semiconductors has been extensively investigated [16]. Recently, Tomás et al. [17] have reported on the influence of the Er^{3+} incorporation into methylene blue-doped CdS thin films. Positions of Er^{3+} into the wurtzite hexagonal CdS lattice have been studied by Watts and Holton [8]. From an extrapolation of these results, it is expected that Er^{3+} enters into Cd^{2+} sites in the zincblende (ZB) cubic CdS lattice, so that *n*-type CdS layers can be obtained. However, it is worth noting that such an assumption is not well understood up to now.

In this study, Er-doped CdS polycrystalline thin films were synthesized by chemical bath deposition (CBD) and their optical and structural properties studied. The optical characterization is performed by photoluminescence and photoacoustic spectroscopy, whereas the structural characterization is carried out by X-ray diffraction (XRD). Similar to the study of Tiwary et al. [18], the enhancement of the infrared PL in a semiconductor due to the incorporation of Er in the lattice, we have observed the same phenomenon in CdS thin films.

Experimental

Polycrystalline CdS thin films were synthesized on glass substrates by CBD at 80 ± 1 °C [19]. The reference chemical bath consisted of 100 mL of an aqueous solution containing $CdCl_2$ (0.02 M), KOH (0.05 M), NH_4NO_3 (1.5 M), and $SC(NH_2)_2$ (0.2 M). Er-doped CdS thin films were then obtained by adding specific volumes (V_{Er}) of an aqueous solution of $Er(NO_3)_3{\cdot}3H_2O$ (0.5 M) to the reference chemical bath (V_{CdS}), so that the total volume $V_t = V_{CdS} + V_{Er}$ was kept constant. The relative volume (V_r), defined as $(V_{Er}/V_t) \times 100\%$, varied from 1 to 10%, in steps of 1% (1 mL), to obtain ten different doping levels. The deposition time was 45 min for all the films. The undoped sample was labeled Er_0, while Er_n with $n = 1,\ldots,10$, stood for the doped samples obtained from chemical baths containing a relative volume of $V_r = n\%$.

The thickness of the films was in the order of 200 ± 10 nm, as determined with a Dektak II profilometer. The structural characterization was carried out with a Siemens D5000 diffractometer, using the CuK_α line. Optical absorption spectra of the films were obtained by Photoacoustic Spectroscopy with a spectrometer fitted with a 1000 W Xenon lamp. The radiation from the lamp was focused onto a variable-frequency light chopper locked at 17 Hz and placed at the entrance slit of a monochromator. The monochromatic light was focused onto the samples placed into a closed photoacoustic cell. The photoacoustic signal was preamplified and then sent to a lock-in amplifier. Dark sheet conductivity (σ) on fresh samples was measured in vacuum, and the sign and concentration of carriers were determined from Hall effect measurements, performed in a conventional apparatus from GMW Magnet Systems model 3472-50. Semi-quantitative measurements of the atomic concentration of elements were achieved by energy dispersive X-ray spectroscopy (EDS) using a Voyager II X-ray quantitative microanalysis in an 1100/1110 EDX system from Noran Instruments, with an uncertainty of ±1%. These measurements indicated that the Cd/S ratio was in the range 1.09–1.02. The Er concentration was determined with an inductively coupled plasma spectrometer ICP Thermo Jarrel Ash model Iris Duo. PL measurements were carried out using the 488 nm Ar^+ laser line, with an average excitation of 40 mW. A cylindrical lens was used to focus the laser beam onto the surface of the sample. The elongated spot had approximated dimensions of 2.5×0.175 mm^2. The PL signal from the sample passed through a Spex 1403 spectrophotometer and was detected with a Hamamatsu R-636 photomultiplier tube. The measurements were taken with aperture slits to achieve a resolution less than 1 cm^{-1}. A phase sensitive technique was used for the PL signal detection, which was implemented using a SRS lock-in amplifier model SR-530. All the PL measurements were carried out at room temperature (RT).

Results and discussion

Shown in Fig. 1 are the X-ray diffraction patterns of the undoped and Er-doped CdS thin films studied. All the diffractograms revealed essentially a peak that, according to the JCPDS file No. 10-454, can be indexed to scattering from the (111) cubic ZB planes. The intensity of this peak reached a maximum value for the sample prepared with $V_r = 2\%$, indicating either the existence of a larger number of (111) planes or that the (111) planes have a lower number of defects. The full width at half maximum (FWHM) of the (111) peak (black diamonds, left axis), as well as the area under the curve of this peak (A_{111}) (white circles, right axis), are plotted as a function of V_r in Fig. 2. While the (111)-FWHM displayed a maximum at $V_r = 3\%$, the area under the curve A_{111} peaked at

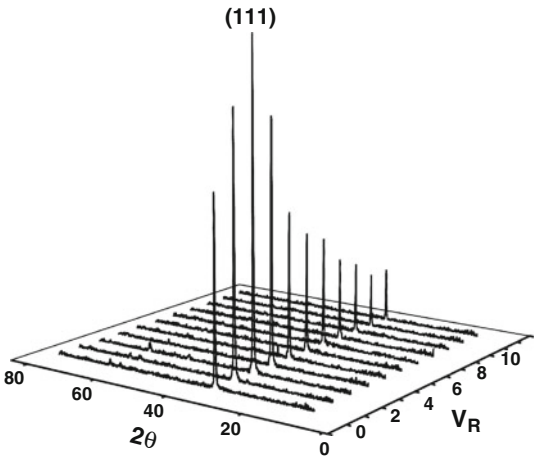

Fig. 1 X-ray diffraction patterns of Er-doped CdS thin films. The peak displayed in the diffractograms, at around $2\theta = 26.5$ degrees, can be indexed to scattering from the (111) cubic zincblende planes

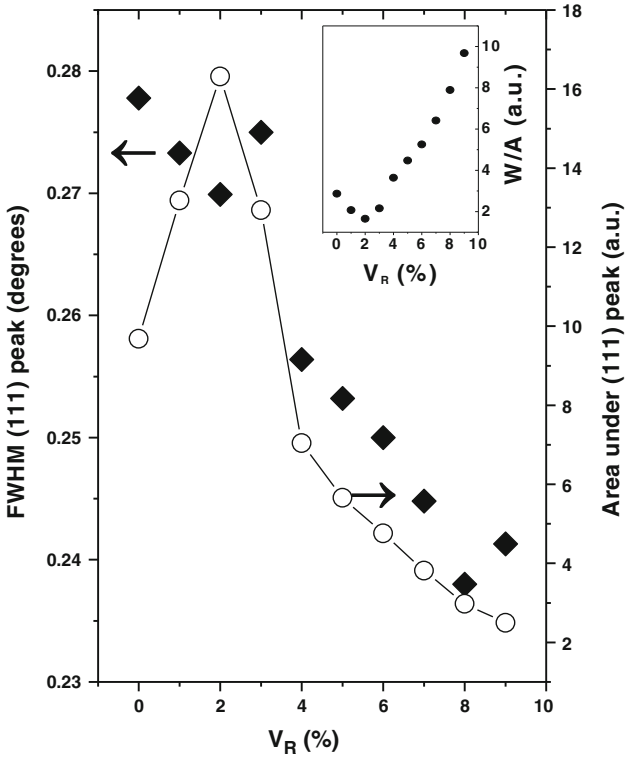

Fig. 2 V_r dependence of the FWHM (*black diamonds*, *left axis*) and the area under the curve (*white circles*, *right axis*) of the (111) peak shown in Fig. 1. The inset exhibits the $FWHM/A_{111}$ ratio as a function of V_r

$V_r = 2\%$. A smaller FWHM is associated with a smaller disorder and hence a better crystalline quality (CQ) of the material; therefore, a plausible figure of merit for the CQ of the material is $FWHM/A_{111}$. The inset of Fig. 2 displays the $FWHM/A_{111}$ data versus V_r. It is observed that the minimum value of $FWHM/A_{111}$ occurs for a relative volume V_r of 2. Accordingly, the best CQ was obtained when $V_r = 2\%$, in agreement with the maximum intensity of the (111) peak.

The incorporation of Er^{3+} (solubility) has been proven more effective in Cd-chalcogenides than in Zn-chalcogenides, a result explained in terms of the cation size [4]. Specifically, the ionic radius of Er^{3+} is 0.89 Å, whereas the ionic radii of Cd^{2+} and Zn^{2+} are 0.95 and 0.74 Å, respectively; the corresponding value for the anion S^{2-} is 1.84 Å. The smaller radius of the triply ionized Er atom thus alters the (111) interplanar distance (ID), giving place to distortion of the ZB–CdS lattice. It has been previously reported that Er^{3+} enters substitutionally into the cation sites in cubic CdTe [20] and ZnSe [21]; in addition, this ion may also enter interstitially into symmetric octahedral interstitial positions in II–VI compounds [9]. Here, we claim that Er^{3+} enters substitutionally into the Cd^{2+} sites of ZB–CdS when low V_r values are used, whereas this ion enters both substitutionally and interstitially into the ZB–CdS lattice for high V_r values. Figure 3 illustrates the dependence of ID on V_r (black circles, right axis). First, the ID decreased with V_r due to the presence of Er^{3+} in substitutional sites, and then the ID increased owing to interstitial Er^{3+}; finally, the ID saturated at $V_r = 6\%$. The ID value estimated for the undoped sample (3.322 Å) resulted shorter than the ID value reported for bulk CdS (3.360 Å), which might be due to both the polycrystalline character of the CdS films and the amorphous nature of the substrate.

From optical absorption measurements, the band-gap energy of the films was obtained. For a direct band-gap semiconductor, such as cubic and hexagonal CdS, the optical absorption in the vicinity of the fundamental absorption edge is described by $[\alpha(hv)*hv]^2 = k\,(hv - E_g)$, where α is the optical absorption coefficient, k is a constant, hv is the energy of the incident photons, and E_g is the band-gap energy. In particular, the absorption spectra were obtained by Photoacoustic Spectroscopy [22]. The V_r dependence of E_g is illustrated in Fig. 3 (white squares, left axis). In accordance with Vegard's law, the dependence of E_g on V_r resembled the opposite behavior of ID as a function of V_r. Accordingly, E_g reached a maximum value (2.45 ± 0.01 eV) at $V_r = 2\%$, decreasing down to 2.37 ± 0.01 eV for $V_r \geq 6\%$.

The inset of Fig. 4 displays the V_r dependence of the atomic concentration of Er, [Er], in atomic percentage, measured in the CdS films by atomic absorption. The approximated linear relationship between [Er] and V_r, calculated by a linear least-squares fit, was $[Er] = (0.11 \pm 0.01)V_r$. In addition, Fig. 4 shows the density of the electrically active Er^{3+} (EAEr) ions measured by the Hall Effect. The sign of the Hall voltage indicates that electrons are the majority carriers. As expected, Er atoms acted as

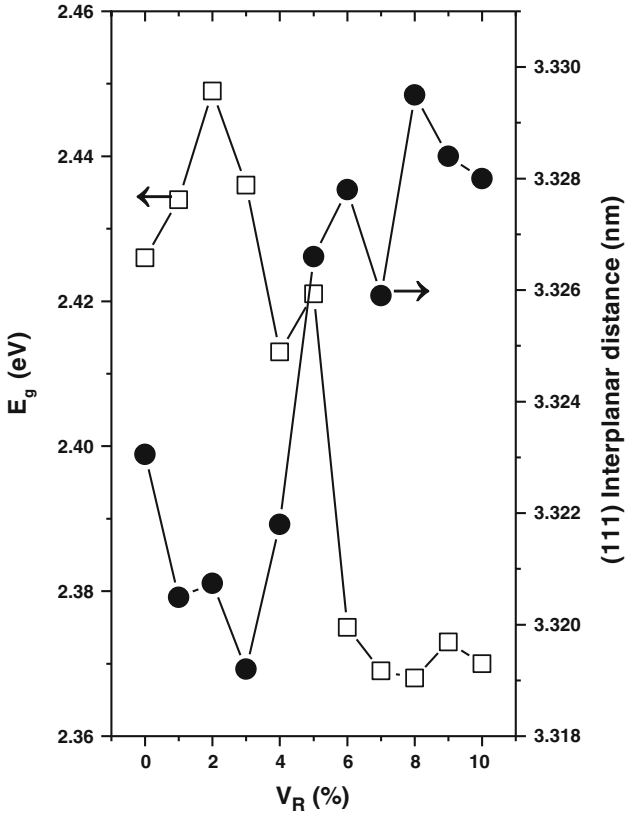

Fig. 3 Dependence of the band-gap energy (*white squares*, *left axis*) and the (111) interplanar distance (*black circles*, *right axis*) on V_r

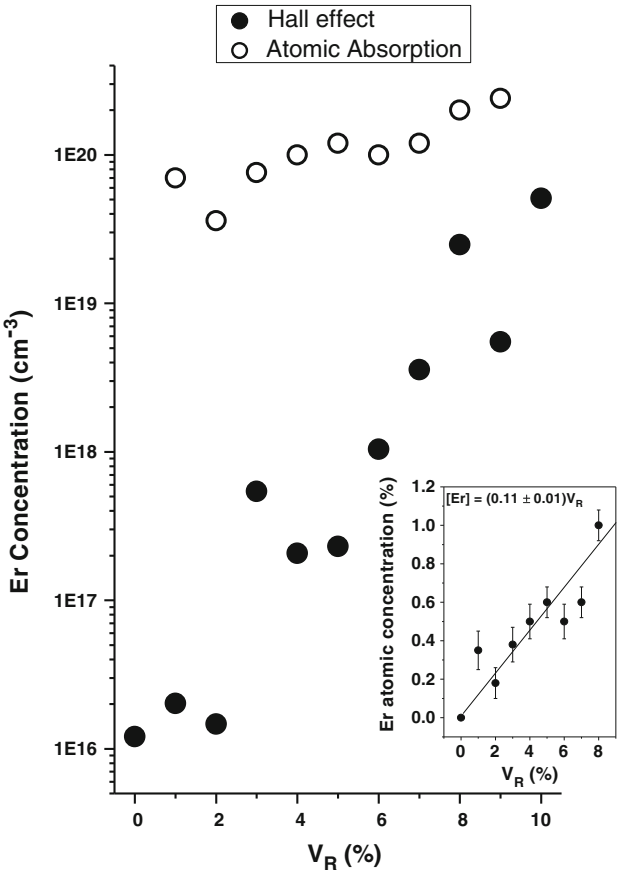

Fig. 4 Logarithm of the Er concentration [Er] in cm^{-3} (*white circles*) and logarithm of the carrier density of electrons (n = [EAEr]) (*black circles*) as a function of V_r. The inset displays [Er] in atomic percentage as a function of V_r

donors. It is assumed that each EAEr ion contributes one free electron to the conduction band (CB) at RT; however, Fig. 4 shows that the density of electrons at the CB, [EAEr] = n, is always smaller than [Er]. The density of active carriers is lower because some Er atoms may be placed interstitially into the CdS lattice, while others may be segregated to grain boundaries; moreover, some Er atoms may also participate in the formation of complexes with vacancies of Cd and (V_{Cd}) and Cd interstials (Cd_I).

Shown in Fig. 5 are the RT-photoluminescence spectra of the whole set of CdS:Er samples. Two main bands are observed: (a) the green emission (GE) band at about 2.4 eV and (b) the band of defects (RE, red emission band) centered at ca. 1.8 eV [18]. On the one side, the GE band has been identified with three types of electronic transitions: (i) CB to shallow acceptor level, (ii) shallow donor level to valence band, and (iii) shallow donor level to shallow acceptor level [23]. On the other side, the RE band which is, in general, associated to defects, in particular, it has been ascribed to surface states originated by S^{2-} vacancies [23–25]. The intensity of both the GE and the RE emission bands is noticeably high for low V_r values, where GE reaches the maximum intensity when $V_r = 1\%$ and RE when $V_r = 2\%$, after that both PL signals gradually lost

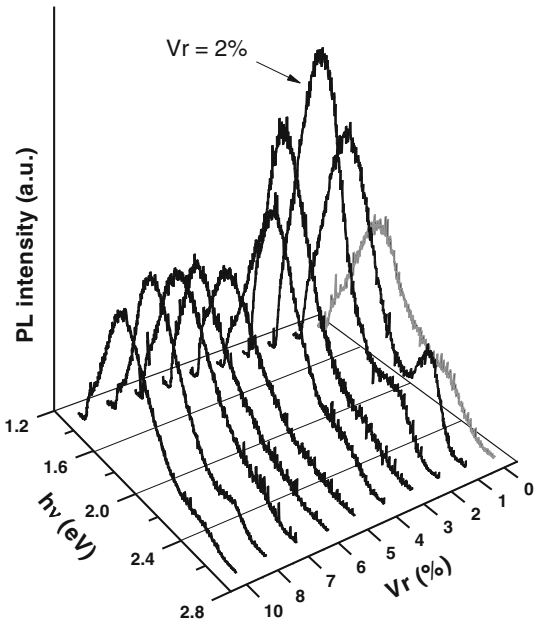

Fig. 5 Photoluminescence spectra of the whole set of the CdS:Er samples

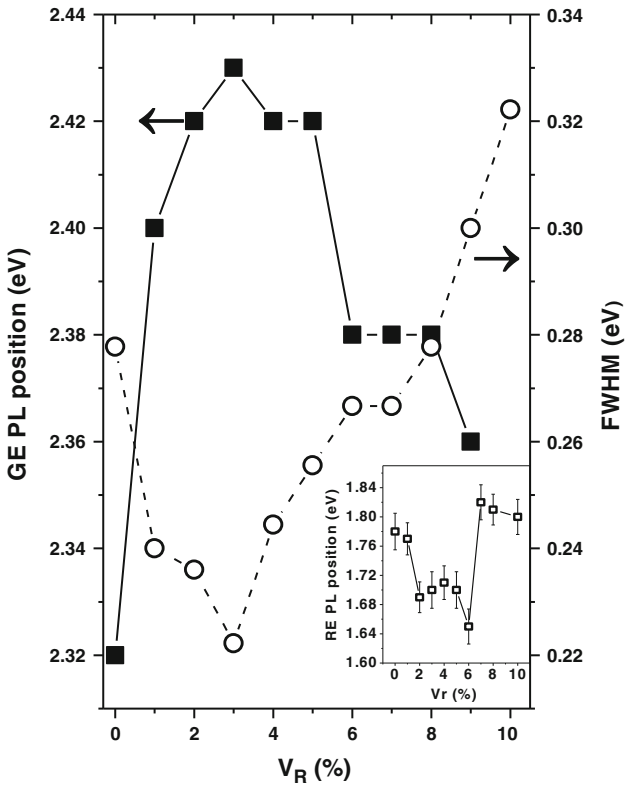

Fig. 6 Energy position (*black squares*, *left axis*) and FWHM (*white* circles, *right axis*) of the GE band as a function of V_r

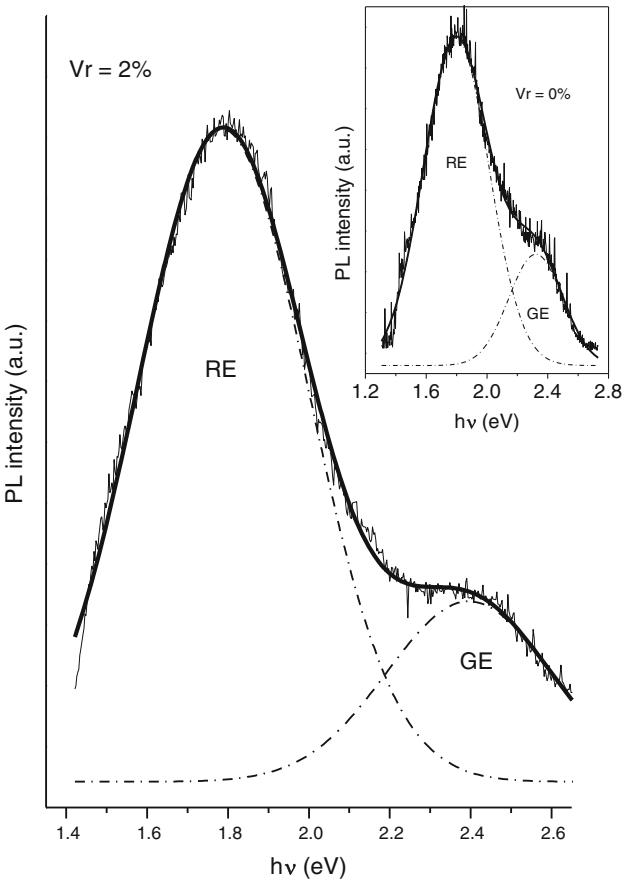

Fig. 7 Deconvolution of the PL spectrum using Gaussian lineshapes for the sample synthesized with $V_r = 2\%$. The inset shows the deconvolution of the PL spectrum for the undoped CdS

intensity and definition as V_r increases. In agreement with Fig. 3, where E_g displays a global maximum by increasing V_r, Fig. 6 shows that the energy center position of the GE band (full squares) initially shifts to higher energies and then it exhibits a red-shift for high V_r values. On the other hand, the RE band displays the opposite behavior (see inset of Fig. 6), shifting initially to lower energies and then showing a blue-shift for high doping levels. Figure 6 also illustrates the FWHM values (open circles) of the GE band as a function of V_r. The maximum energy position of the GE band took place at $V_r = 3\%$, shifting approximately 0.11 eV with respect to the undoped film. The behavior of the FWHM confirms that the CQ of the material is better for low doping levels, in agreement with the XRD measurements. The GE band shows a dependence on V_r similar to that of CQ and opposite to that shown by ID (see inset of Figs. 2 and 3)

The PL spectra were deconvoluted using Gaussian lineshapes as illustrated in Fig. 7 for the film deposited with a $V_r = 2\%$. As expected, two bands are fitted: the GE band and the RE band. The inset in Fig. 7 shows the GE and RE deconvolution of the PL spectrum for the undoped sample ($V_r = 0\%$). However, for $V_r \geq 3\%$, the deconvolution process requires in almost all cases the fitting to three Gaussian lines, a third band appears at about 2.2 eV: a yellow band (YE), Fig. 8 shows the PL deconvolution for $V_r = 7\%$ and the inset for $V_r = 3\%$ using three Gaussian lineshapes. The YE PL band has been correlated with V_{Cd}'s and complexes involving this punctual defect [26], and with V_{Cd}–Cd_I complexes [27, 28]. When Er^{3+} ions enter in Cd sites substituted Cd^{2+} ions, then in order of the charge neutrality, and by considering that CdS is a more ionic than covalent material, V_{Cd}'s must be generated. The process involves the formation of a Cd_I defect density also. In this way, for large V_r values, the existence of YE band can be expected in the PL spectra of CdS. The lattice of CdS degenerates with the presence of large Er concentrations, whether in interstitial positions or giving place to other structural complexes, in such a way that the PL efficiency is degraded.

Finally, the RT-dark conductivity σ was measured with the purpose to confirm the improvement of the CQ for low V_r values. The inset of Fig. 9 displays σ as a function of V_r. The mobility (μ) can be determined from the relationship $\sigma = e\mu n$, where e is the charge of the electron, and n is the Er concentration plotted in Fig. 4. Figure 9 shows the dependence of μ on V_r. As expected, the maximum value of

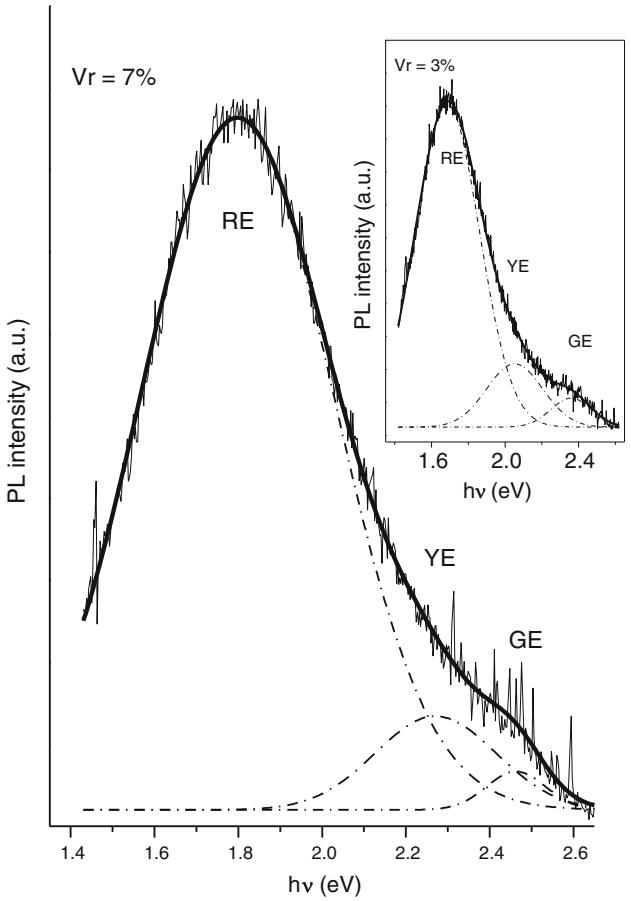

Fig. 8 Deconvolution of the PL spectrum using Gaussian lineshapes for the sample synthesized with $V_r = 7\%$. The inset shows the deconvolution of the PL spectrum for $V_r = 3\%$

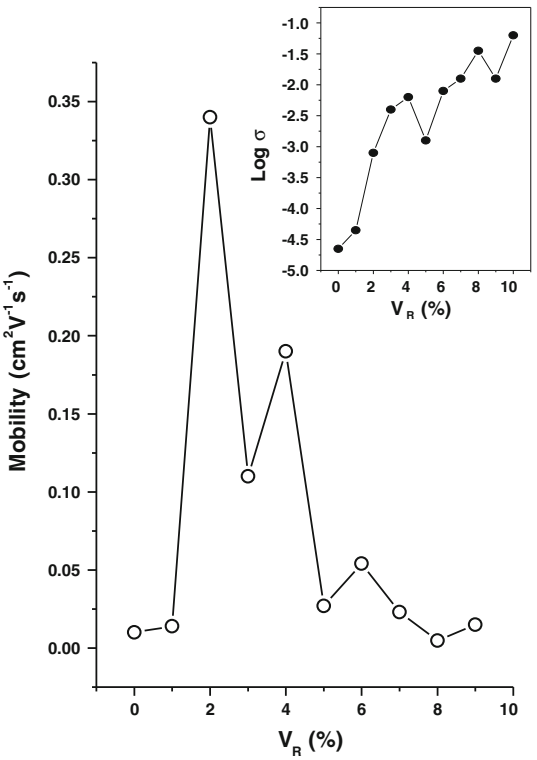

Fig. 9 Dependence of the electron mobility on V_r. The error bar is about 20% for the all experimental points. The inset shows the logarithm of σ at RT as a function of V_r

μ occurred for $V_r = 2\%$, in agreement with the fact that the better the CQ the larger the mobility. Recalling the competition between the crystal quality, the photoluminescence, and the electrical conductivity, Fig. 9 indicates that a large CQ implies low σ values and vice versa.

Conclusion

A simple procedure to introduce Er^{+3} ions into the core of CdS films, without large damage of the lattice (E_g decreases only 2%), has been presented. Er-doping was carried out chemically during the growth process by adding controlled volumes (V_r) of an Er reagent in the growing solution. Maxima values of $n = 5.2 \times 10^{19}$ cm^{-3} and $\sigma \cong 0.1\ \Omega^{-1}$ cm^{-1} were reached for the sample synthesized at a $V_r = 10\%$. The forbidden gap energy decreased down to 2.37 eV for the samples synthesized with a $V_r \geq 6\%$. The PL spectra displayed emissions attributed to both the host material and the doping agent. The minimum ID, the best CQ, and consequently the most intense PL emissions, as well as the maximum GE blue-shift were obtained for $V_r = 2\%$, showing that Er-doped CdS thin films prepared under these conditions have a potential use in optoelectronic applications.

Acknowledgements The authors are grateful to M. Guerrero, A. Soto, M. Becerril, and S. V. Miranda for their technical assistance. This study was partially supported by CONACyT (Mexico).

References

1. Zhang X, Li L, Huang Q, Zhang Z, Xi Q, Dong X, Liu Y, Ji T (2010) Nanosci Technol 10:5288
2. Choi MH, Ma TY (2008) Mater Lett 62:1835
3. Fuhisawa M, Asakura A, Elmasry F, Okubo S, Ohta H, Fujiwara Y (2010) J Phys Condens Matter 200:062005
4. Krasilnik ZF, Andreev BA, Kryzhkov DI, Krasilnikova LV, Kutznetsov VP, Yu D, Shmagin VB, Gregorkievicz T, Vinh NQ, Jantsch W, Przybylinska H, Timoshenko VY, Zhigunov DN (2006) J Mater Res 21:574
5. Shen H, Pamulapati J, Taysing M, Wood MC, Lareau RT, Ervin MH, Mackenzie JD, Abernathy CR, Pearton SJ, Ren F, Zavada JM (1999) Solid State Electron 43:1231
6. Gregorkiewicz T, Thao DTX, Langer JM (1999) Appl Phys Lett 75:4121
7. Xiang Q, Zhou Y, Ooi BS, Lam YL, Chan YC, Kam CH (2000) Thin Solid Films 370:243
8. Watts RK, Holton WC (1968) Phys Rev 173:417

9. Boyn R (1988) Phys Status Solidi B 148:11
10. Dziesiaty J, Muller S, Boyn R, Buhrow T, Klimakow A, Kreissl J (1995) J Phys Condens Matter 7:4271
11. Georgobiani AN, Kotljarevsky MB, Kidalov VV, Rogozin IV, Aminov UA (2000) J Cryst Growth 214:516
12. Schmidt T, Muller G, Spanhel L, Kerkel K, Forchel A (1998) Chem Mater 10:65
13. Favennec PN, L'Haridon H, Salvi M, Moutonnet D, Le Guillou Y (1989) Electron Lett 25:718
14. Zelaya-Angel O, Alvarado-Gil JJ, Lozada-Morales R, Vargas H, Da Silva A (1994) Appl Phys Lett 64:291
15. Tomás SA, Vigil O, Alvarado-Gil JJ, Lozada-Morales R, Zelaya-Angel O, Vargas H, Da Silva AF (1995) J Appl Phys 78:2204
16. Tomás SA, Stolik S, Altuzar V, Zelaya O, Lozada R, Carmona JJ, Portillo O, Davila JA (2003) Rev Sci Instrum 74:569
17. Tomás SA, Lozada-Morales R, Portillo O, Lima–Lima H, Palomino-Merino R, Zelaya O (2008) Eur Phys J Special Topics 153:299
18. Tiwary M, Singh NK, Annapoorni S, Agarwal DC, Avasthi DK, Mishra YK, Mazzoldi P, Mattei G, Sada C, Trave E, Battaglin G (2011) Vacuum 85:806
19. Martinez-Montes JL, Martinez G, Torres-Delgado G, Guzmán O, Zelaya-Angel O, Lozada-Morales R (1996) J Mater Sci Mater Electron 8:72
20. Title RS, Crowder BL, Mayo JW (1967) In: Thomas DG (ed) II-VI semiconducting compounds. Benjamin, New York
21. Kingsley JD, Aven M (1967) Phys Rev 155:235
22. Tomás SA, Stolik S, Palomino R, Lozada R, Persson C, Pepe A, Ferreira da Silva A (2005) J Appl Phys 98:073516
23. Lozada-Morales R, Zelaya-Angel O, Torres-Delgado G (2001) Appl Surf Sci 175/176:62
24. Kulp BA, Kelley RH (1960) J Appl Phys 31:1057
25. Achour S, Talat GH (1986) Thin Solid Films 144:1
26. Artem'jeva OO, Vakulenko OV, Dacenko OI (2005) Semicond Phys Quantum Electron Optoelectron 8:58
27. Abken AE, Halliday DP, Durose K (2009) J Appl Phys 105: 064515
28. Lozada-Morales R, Zelaya-Angel O, Torres-Delgado G (2001) Appl Phys A 73:61